Comparison of the Binding Sites for High-Potential Iron−Sulfur Protein and Cytochrome *c* on the Tetraheme Cytochrome Subunit Bound to the Bacterial Photosynthetic Reaction Center†

Artur Osyczka,‡,§ Kenji V. P. Nagashima,‡ Satoshi Sogabe,||,⊥ Kunio Miki,|| Keizo Shimada,‡ and Katsumi Matsuura*,‡

Department of Biology, Tokyo Metropolitan University, Minamiohsawa 1-1, Hachioji, Tokyo 192-0397, Japan, and Department of Chemistry, Graduate School of Science, Kyoto University, Sakyo-ku, Kyoto 606-8502, Japan

Received April 21, 1999; Revised Manuscript Received August 16, 1999

ABSTRACT: A tetraheme cytochrome subunit bound to the photosynthetic reaction center (RC) of purple bacterium, *Rubrivivax gelatinosus*, interacts with two types of soluble electron donors, cytochromes *c* and high-potential iron−sulfur protein (HiPIP), at a binding domain in the vicinity of low-potential heme 1, the fourth heme from the special pair of bacteriochlorophyll. To clarify the mechanism of the interaction, the domain around heme 1 was examined using site-directed mutants that changed the surface charge in the region within 20 Å from the heme edge. In the case of the interaction with soluble cytochrome *c*, a strong dependence on the sign of the introduced charge was observed in all mutants: positive charge inhibited the reaction rate, whereas additional negative charge accelerated it. This confirmed the electrostatic nature of the binding. Interaction with HiPIP was inhibited by a limited number of mutations at the close vicinity of heme 1, and no acceleration was observed (the effects of some mutations were independent of the sign of the introduced charge). The acidic residues which were critically important for the binding of cytochrome *c* showed much less contribution to the binding of HiPIP. The binding site for HiPIP appears to be mostly formed by uncharged and hydrophobic residues, occupying a significantly smaller area than the cytochrome-*c*-binding site. It is proposed that the docking of HiPIP to the RC in *Rvi. gelatinosus* is primarily controlled by hydrophobic contacts between protein surfaces, thus differing from the electrostatic mode of the RC-cytochrome *c* interaction.

Transient and specific interactions between proteins play important roles in many biological reactions. The steric and electrostatic properties of the interacting surfaces of the proteins are thought to determine the ability of proteins to recognize one another and form specific associations. The functional integrity of both respiratory and photosynthetic chains is based on the effectiveness of mobile electron carriers to transfer electrons from one membranous complex to another. Therefore, many studies have been dedicated to elucidating the molecular basis of the selectivity of the interactions between small, water-soluble proteins and large, transmembrane complexes in various physiological and nonphysiological systems.

A useful model to study these types of interactions is offered by a photosynthetic reaction center from purple bacteria (RC)[1]—an integral membrane protein complex mediating primary processes of photosynthesis. In this system, soluble electron carrier proteins engage in the process of rereduction of the oxidized special pair of bacteriochlorophyll (P^+) generated in the RC upon the light-induced primary charge separation. In most species of purple bacteria, the reduction of P^+ is initially performed by the hemes of the RC-bound tetraheme cytochrome subunit, which then accept electrons from soluble electron carriers (reviewed in refs *1* and *2*). Some species, on the other hand, do not have the tetraheme subunit associated with the RC. In these cases, a soluble electron carrier (cytochrome c_2) acts as an immediate electron donor to P^+ (reviewed in refs *2*−*4*).

The interaction between cytochrome c_2 and the RC without a bound tetraheme subunit is electrostatic in nature and occurs through the formation of salt bridges between lysine residues encircling the heme crevice of cytochrome c_2 and negatively charged carboxylate groups surrounding P on the periplasmic surface of the RC (*5*−*9*).

Our recent study with the *Rubrivivax gelatinosus* RC showed that the interaction between soluble electron donors and the RC with a bound tetraheme cytochrome subunit occurs in the region near the exposed edge of the low-

† This work was supported in part by a grant-in-aid from the Ministry of Education, Science and Culture, Japan (0904423) and a special grant (1999) from Tokyo Metropolitan University.

* To whom correspondence should be addressed. Phone: (+81) (426) 77 2582. Fax: (+81) (426) 77 2559. E-mail: matsuura-katsumi@c.metro-u.ac.jp.

‡ Tokyo Metropolitan University.

§ Permanent address: Institute of Molecular Biology, Jagiellonian University, Krakow, Poland.

|| Kyoto University.

⊥ Present address: Nippon Roche Research Center, Department of Chemistry, Kajiwara 200, Kamakura, Kanagawa 247-8530, Japan.

[1] Abbreviations: RC, reaction center; HiPIP, high-potential iron−sulfur protein; E_m, redox midpoint potential; P, special pair of bacteriochlorophyll; P^+, oxidized state of P; DAD, 2,3,5,6-tetramethylphenylenediamine; PCR, polymerase chain reaction; PS I, photosystem I.

10.1021/bi990907d CCC: $18.00
Published on Web 11/06/1999

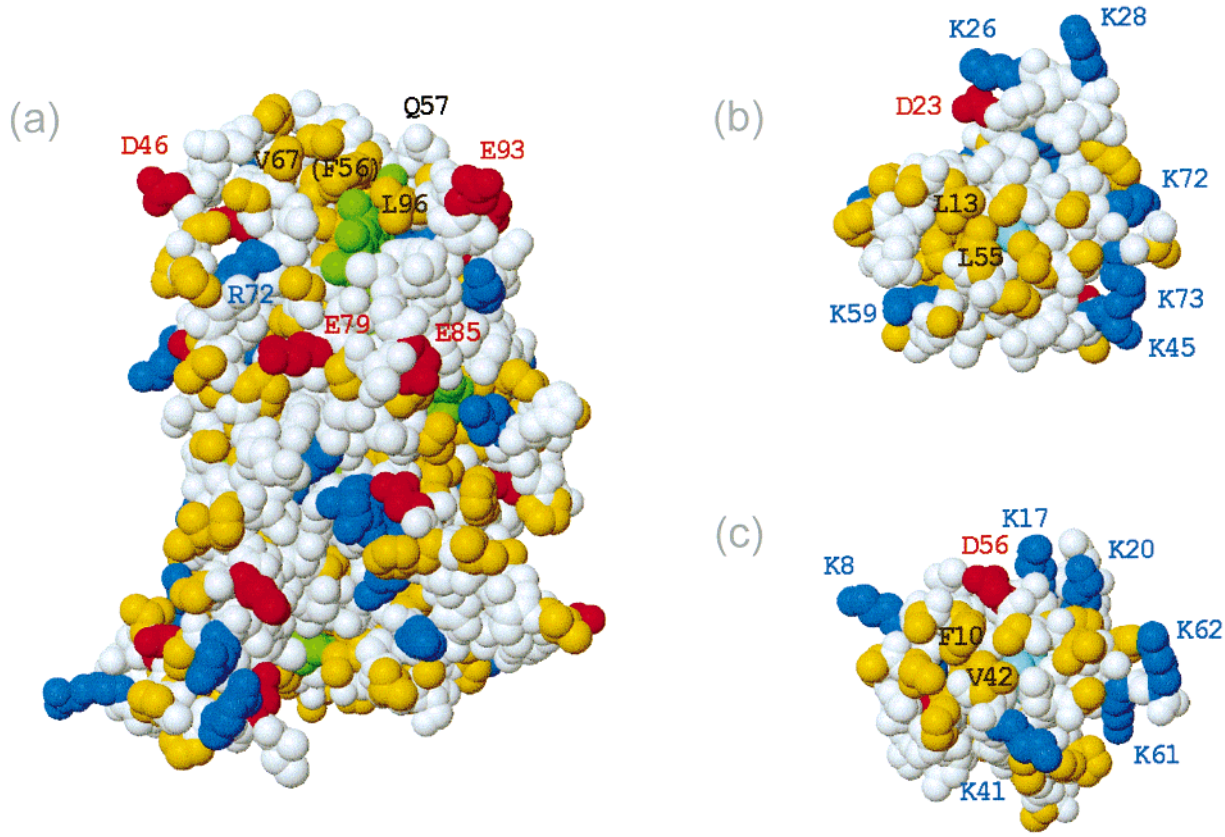

FIGURE 1: Left: (a) space-filling representation of the modeled structure of *Rvi. gelatinosus* RC-bound cytochrome subunit (built on the basis of the crystallographic structure of *Blc. viridis* RC as described in ref *10*). The heme groups are *c*-551 (heme 1, E_m = 70 mV), *c*-555 (heme 2, E_m = 300 mV), *c*-551 (heme 4, E_m = 130 mV), *c*-555 (heme 3, E_m = 320 mV), from top to bottom. Heme 3 is closest to P. Mutated were all marked residues (except for the position in parentheses). Right: (b) front side of the modeled structure of *Rvi. gelatinosus* HiPIP (built on the basis of the crystallographic structure of *Ect. vacuolata* HiPIP as described in Materials and Methods); (c) front side of the crystallographic structure of *Rcy. tenuis* HiPIP. Color code: Asp, Glu (red); Lys, Arg (blue); Ala, Val, Ile, Leu, Met, Pro, Phe (yellow); heme (green); iron−sulfur cluster (cyan). The figure was generated using the programs MOLSCRIPT (*56*) and RASTER3D (*57*).

potential heme 1 (*c*-552, E_m = 70 mV) of the subunit, the most distant heme from P (*10*, *11*). With respect to the known three-dimensional structure of the *Blastochloris* [formerly called *Rhodopseudomonas* (*12*)] *viridis* RC (*13*−*15*), the determined site of interaction corresponds to a region near heme *c*-554 (E_m = −60 mV) of the cytochrome subunit (*16*), the region that has been considered as a possible binding site for cytochrome c_2 (*17*).

The identification of the binding site in *Rvi. gelatinosus* was based on a newly developed gene-transfer system which permitted the obtaining of mutants expressing the RCs with a genetically modified cytochrome (*10*). The substitutions of negatively charged glutamic or aspartic acids with lysines or histidines in the region near heme 1 (mutations at positions E93, E79, E85, and D46; see Figure 1a) revealed that soluble cytochromes, upon binding to the RC, recognize the cluster of acidic residues encircling this heme (*10*). The inhibitory effects observed for the single- and double-charge substitutions were consistent with the electrostatic mode of the binding (interactions between lysines of soluble cytochromes and the carboxylate groups of the membranous partner). The site near heme 1 appeared to be a unique docking site for cytochromes, as all other tested regions of the subunit showed no involvement in the RC-cytochrome *c* interaction.

The region near heme 1 was also identified as a binding site for high-potential iron−sulfur protein (HiPIP), the main physiological electron donor to the *Rvi. gelatinosus* RC (*18*). The interaction with HiPIP was found to be considerably impaired by the removal of the acidic cluster from the region (the triple mutation E79K/E85K/E93K) and the mutation in the hydrophobic domain near the heme pocket (the single mutation at position V67, see Figure 1a) (*11*). However, mutation V67K resulted in a much more pronounced effect than an almost complete lack of negative charge in the region. This specific order of the inhibition, which was different from that obtained with cytochrome *c*, indicated that the binding of HiPIP to the RC and the binding of cytochrome *c* to the RC may primarily be controlled by different sets of amino acids. This suggested the possible existence of considerable differences not only in the configurations of the transient complexes but also in the binding mechanism itself.

The present work shows further details of the HiPIP−RC interaction and the cytochrome *c*-RC interaction to gain more insights into how these two types of soluble electron donors associate with the RC-bound tetraheme cytochrome subunit. With the use of additional point mutations generated in the region near the exposed heme 1 of the subunit, we define more precisely the domains responsible for the binding of HiPIP and cytochrome *c* and compare their relative positions with respect to the heme crevice. We also discuss the differences in the kinetic behaviors of HiPIP and cytochrome *c* with respect to the possible docking mechanisms.

MATERIALS AND METHODS

Preparation of RC Site-Directed Mutants. *Rvi. gelatinosus* strains with the mutated RC-bound tetraheme cytochrome subunit were generated and analyzed as described in ref *10*. Site-specific mutagenesis was performed on the basis of the Kunkel method, as implemented in the Mutan-K mutagenesis kit (Takara Shuzo Co., Ltd.), using the pGI7-1 plasmid (*10*) as the template DNA. The following oligonucleotides were used to introduce single mutations: 5′-CTTGACGTTCTT-GAACACCTGGTTG-3′ for Q57K; 5′-CGTGAACTCCGC-TTCCGACAGATG-3′ for V67E; 5′-CGCCATCTGCTC-CGTGAACTC-3′ for R72E; 5′-AGTCGTCGGCCTTGTTCT-CGGTATG-3′ for L96K (mismatch positions are underlined). A template with the double-point mutation V67E/R72E was constructed by the addition of a single mutation R72E to the pGI7-1 plasmid containing the mutation V67E. Other oligonucleotides are described in refs *10* and *11*. Mutations and the sequence integrity of the entire *puf*C gene were further confirmed by DNA sequence analysis. The mutated pGI7-1 plasmids were incorporated into the genomic DNA of the ΔC strain (*puf*C-gene deletion background) (*10*), and the presence of desired mutations was confirmed by DNA sequence analysis of the *puf*C gene amplified by PCR from the genomic DNA of mutated strains.

Membranes, Proteins, and Kinetic Measurements. Membrane fractions containing the wild-type and mutated RC complexes were prepared as described in refs *10* and *19*. *Rvi. gelatinosus* HiPIP was isolated and purified as described in ref *19*. *Rcy. tenuis* HiPIP was isolated and purified as described in ref *20*. Horse mitochondrial cytochrome *c* (type VI) was from Sigma.

Xenon-flash-induced absorbance changes accompanying electron transfer were recorded using a single-beam spectrophotometer assembled in our laboratory (*21*). Experiments were performed aerobically in 10-mm-path-length cuvettes with 2 mM Mops-NaOH (pH 7) (for the reaction with HiPIP) or 2 mM Tris-HCl (pH 8) (for the reaction with cytochrome *c*) containing 20 μM DAD and 0.1 mM sodium ascorbate. The concentration of membranes was adjusted to $A_{850} = 1.0$ (approximately 0.1 μM RC). The reduction of the bound cytochrome was followed by monitoring at wavelengths of 555 or 556 nm for the reaction with HiPIP or cytochrome *c*, respectively.

Homology-Model Building and Manual Docking Simulation. The model of the cytochrome subunit of the *Rvi. gelatinosus* RC was build based on the coordinates of the *Blc. viridis* RC, as described in ref *10*. The model of *Rvi. gelatinosus* HiPIP was built using the same procedures. *Ectothiorhodospira vacuolata* HiPIP (*22*; protein data bank entry 1HPI) was selected from the structure-solved HiPIPs as a template model because of similar polypeptide chain length and relatively high sequence similarity (*23*). The protein folding of the three-residue insertion (residues 28−30) in comparison with *Ect. vacuolata* HiPIP was built on the basis of the crystal structure of *Chromatium purpuratum* HiPIP (*24*).

The putative docking model between HiPIP and the RC-bound cytochrome subunit was manually built using the same procedures as described in ref *10* using the program MOLOC (*25*). *Rhodocyclus tenuis* HiPIP (*26*) was chosen as a counterpart of the RC since the region of the insertion (residues 22−31; upper region in Figure 1b) in *Rvi. gelatinosus* HiPIP remains structurally ambiguous. In this region, polypeptide chain lengths and amino acids are various among HiPIPs. HiPIP and the RC were mutually orientated to interact with each hydrophobic patch on the surface, with some reorientation of the side chains of the surface residues. Finally, interatomic distances were checked to ensure that no van der Waals overlap occurred between atoms at the intermolecular interface, and the contact surface area was estimated using a solvent-accessible surface (*27*) by a 1.4 Å probe sphere.

RESULTS

Mutational Amino Acid Changes on the Surface of Cytochrome Subunit. The series of the mutants of the tetraheme cytochrome subunit used in this study was designed to examine the protein surface participating in the binding of soluble protein partners. Following previous studies, which showed that the vicinity of the solvent-exposed edge of the low-potential heme 1 is involved in this process (*10, 11*), all mutants presented in this work have surface amino acid substitutions in the region around heme 1.

The positions of the mutated residues are shown in Figure 1a. The acidic residues, which form a cluster surrounding heme 1, were replaced either by lysine or histidine. These replacements included single (E85K, E79K, E93K, and D46H), double (E79K/E85K and E93K/E85K), and triple (E79K/E85K/E93K) mutations, and resulted in a progressive decrease of negative charge concomitant with an increase of positive charge on the surface of the interacting site.

The hydrophobic domain immediately surrounding the heme crevice was mutated at positions V67 and L96 by introducing either positively or negatively charged polar residues (V67K, L96K or V67E, respectively). The polar but uncharged position in the region adjacent to the hydrophobic domain was replaced by lysine (Q57K). An additional negative charge was introduced to the binding domain by replacing R72 with glutamate (R72E). The two single mutants (V67E and R72E) and the double mutant V67E/R72E enhanced the negative charge already existing in the region as a result of the acidic cluster present in the native protein.

To examine whether the site-specific mutants of the surface amino acids still have wild-type properties with respect to electrochemistry and structure, we compared the redox titrations of the mutant and wild-type membranes (data not shown). No differences were observed between the wild-type and three mutants, V67K, V67E/R72E, and E79K/E85K/E93K. These mutants were chosen since they showed large effects on the reaction rates with soluble electron donors (see below). Two low-potential hemes showed the midpoint potentials (pH 8.0) of around 50 mV and two high-potential hemes, around 320 mV in all strains examined. (Further resolution of two low- and two high-potential hemes was unsuccessful in the membrane preparations, probably due to the relatively large overlap of carotenoids in the spectral region of the α-band of hemes and to interference from other minor *c*-type hemes.) These results suggest that there are no major effects of the mutations introduced to the surface amino acids on the redox potentials of hemes and basic structure of the subunits.

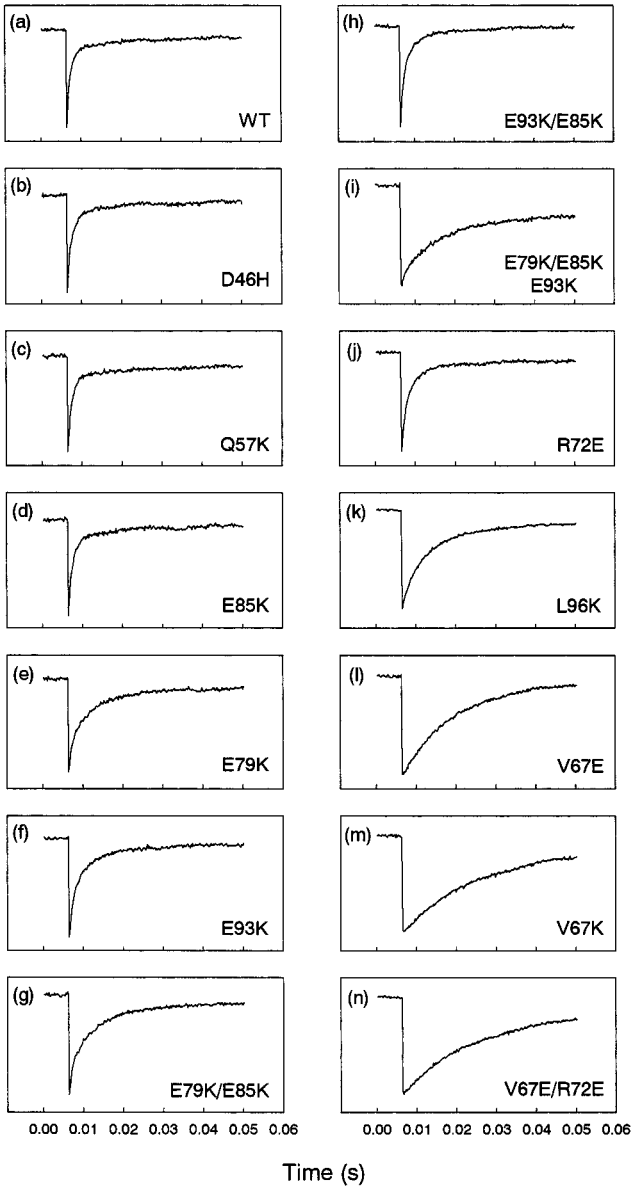

FIGURE 2: Single-flash-induced oxidation and reduction of RC-bound hemes measured at 555 nm for the reaction of wild-type (a) and mutated (b−n) tetraheme cytochrome subunits of *Rvi. gelatinosus* RC with 3 μM *Rvi. gelatinosus* HiPIP. All traces are plotted on the same time resolution scale. The height of each panel corresponds to ΔABS of 2.0×10^{-3}. Buffer solution contained 2 mM Mops−NaOH (pH 7), 20 μM DAD and 0.1 mM sodium ascorbate.

RC Mutants in the Reaction with Rvi. gelatinosus HiPIP. Kinetic traces at 555 nm for the reaction of *Rvi. gelatinosus* HiPIP with wild-type and mutants of the RC-bound cytochrome subunit presented in Figure 2 show the flash-induced photooxidation of a bound cytochrome (downward signal in submilliseconds) followed by its rereduction by HiPIP (absorbance increase within tens of milliseconds). The second-order rate constants for the reduction of the wild-type and mutated RCs in the presence of HiPIP are summarized in Table 1.

At low ionic strength, the kinetic behavior of individual mutants falls into three categories. The first group of mutants includes those which were reduced with the same rate as the wild-type [$k = (2.6-2.8) \times 10^8$ M^{-1} s^{-1}]. These mutants were D46H, Q57K, and E85K (Figure 2, panels b−d). The second group includes mutants which, in comparison to the wild-type, showed small inhibitory effects. These were single mutants at positions E79, E93, and R72 (Figure 2, panels e, f, and j, respectively), and double mutants E79K/E85K and E93K/E85K (Figure 2, panels g and h, respectively). Minor differences in the effects of these mutants are recognizable: the effect caused by E79K ($k = 1.1 \times 10^8$ M^{-1} s^{-1}) was slightly larger than that caused by either E93K or R72E ($k = 2.3 \times 10^8$ M^{-1} s^{-1}). The double mutants E79K/E85K and E93K/E85K reacted with the same rates as single mutants E79K and E93K, respectively.

The third group consists of single mutants at positions L96 and V67, double mutant V67E/R72E, and triple mutant E79K/E85K/E93K, all of which showed strong inhibition of the reaction with HiPIP. Single mutant L96K reacted with the rate of 7.3×10^7 M^{-1} s^{-1} (Figure 2k). The triple mutant E79K/E85K/E93K (Figure 2i) reacted more slowly than L96K, with a rate of 5.6×10^7 M^{-1} s^{-1}. The largest single-position inhibition was observed for V67 (V67E and V67K shown in Figure 2, panels l and m, respectively). Interestingly, inhibition at this position was independent of the sign of the introduced charge, i.e., oppositely charged amino acids (lysine and glutamate) produced a similar inhibitory effect, slightly larger in the case of lysine ($k = 1.6 \times 10^7$ M^{-1} s^{-1}) than in the case of glutamate ($k = 3.0 \times 10^7$ M^{-1} s^{-1}). Double mutant V67E/R72E (Figure 2n) resulted in additive inhibition as compared to the single mutants V67E and R72E ($k = 1.1 \times 10^7$ M^{-1} s^{-1}).

The effect of ionic strength on the second-order rate constant for the reaction of HiPIP with wild-type and mutated cytochrome subunits is presented in Figure 3. In all cases, the solid lines were obtained, applying the parallel plate model of Watkins et al. (*28*) as described in ref *10*. The wild-type cytochrome shows a marked ionic strength dependence. The rate of its reaction with HiPIP decreases over 1 order of magnitude with increasing salt concentration and the best-fit yields the value of a second-order rate constant at infinite ionic strength $k_\infty = 1.1 \times 10^7$ M^{-1} s^{-1} and a radius of the interaction site $R = 19$ Å.

Mutants D46H, Q57K, and E85K exhibited the same ionic strength dependency as the wild-type, yielding similar values of k_∞ (Table 1). The mutants at positions E79 and E93 displayed small but recognizable changes, i.e., k_∞ for E93K was a little lower than the wild-type value (Table 1) and the curve for E79 was slightly less steep than that of the wild-type (Figure 3A). Double mutants E79K/E85K and E93K/E85K showed the same dependency as single mutants E79K and E93K, respectively (Table 1). The ionic strength dependency of the triple mutant E79K/E85K/E93K was less steep (Figure 3A), but its reactivity at high ionic strength (k_∞) was not changed in comparison with the wild-type.

In contrast to the mutants at positions E79 and E93, which displayed a kinetic behavior at high ionic strength similar to this of the wild-type, the mutants grouped in Figure 3B exhibited a dramatic decrease in the rates with increasing salt concentration. At higher ionic strength, their reactivity dropped to a much lower level than that of the wild-type. This phenomenon was observed in single mutants R72E, L96K, V67E, and V67K and double mutant V67E/R72E. The extent of the decrease in the reactivity was site-specific (Table 1). The highest value of k_∞ in this group observed for R72E ($k_\infty = 1.0 \times 10^6$ M^{-1} s^{-1}) was 1 order of magnitude

Table 1: Second-Order Rate Constants (k) and the Rates at Infinite Ionic Strength (k_∞) for the Reaction of *Rvi. gelatinosus* HiPIP and *Rcy. tenuis* HiPIP with Wild-Type and Mutants of *Rvi. gelatinosus* RC-Bound Tetraheme Cytochrome Subunit

	Rvi. gelatinosus HiPIP		*Rcy. tenuis* HiPIP	
RC	k (M^{-1} s^{-1})[a]	k_∞ (M^{-1} s^{-1})[b]	k (M^{-1} s^{-1})[a]	k_∞ (M^{-1} s^{-1})[b]
WT	2.8×10^8	1.1×10^7	8.0×10^6	1.3×10^6
D46H	2.6×10^8	9.7×10^6	9.0×10^6	1.6×10^6
Q57K	2.7×10^8	1.0×10^7	7.8×10^6	1.4×10^6
E85K	2.8×10^8	1.2×10^7	7.0×10^6	1.4×10^6
E79K	1.1×10^8	1.1×10^7	5.0×10^6	1.3×10^6
E93K	2.3×10^8	8.5×10^6	3.4×10^6	1.0×10^6
E79K/E85K	1.2×10^8	1.1×10^7	4.0×10^6	1.4×10^6
E93K/E85K	2.3×10^8	8.1×10^6	2.5×10^6	9.6×10^5
E79K/E85K/E93K	5.6×10^7	1.0×10^7	1.2×10^6	6.9×10^5
R72E	2.3×10^8	1.0×10^6	7.2×10^6	6.5×10^5
L96K	7.3×10^7	5.2×10^5	1.0×10^6	3.2×10^5
V67E	3.0×10^7	1.3×10^5	1.5×10^6	2.1×10^5
V67K	1.6×10^7	2.0×10^5	1.4×10^6	2.0×10^5
V67E/R72E	1.1×10^7	7.0×10^4	1.5×10^6	6.5×10^4

[a] Measured in 2 mM Mops-NaOH, pH 7. [b] The rate constants at infinite ionic strength (k_∞) were calculated applying the parallel plate (Watkins) model for protein−protein interactions (*28*).

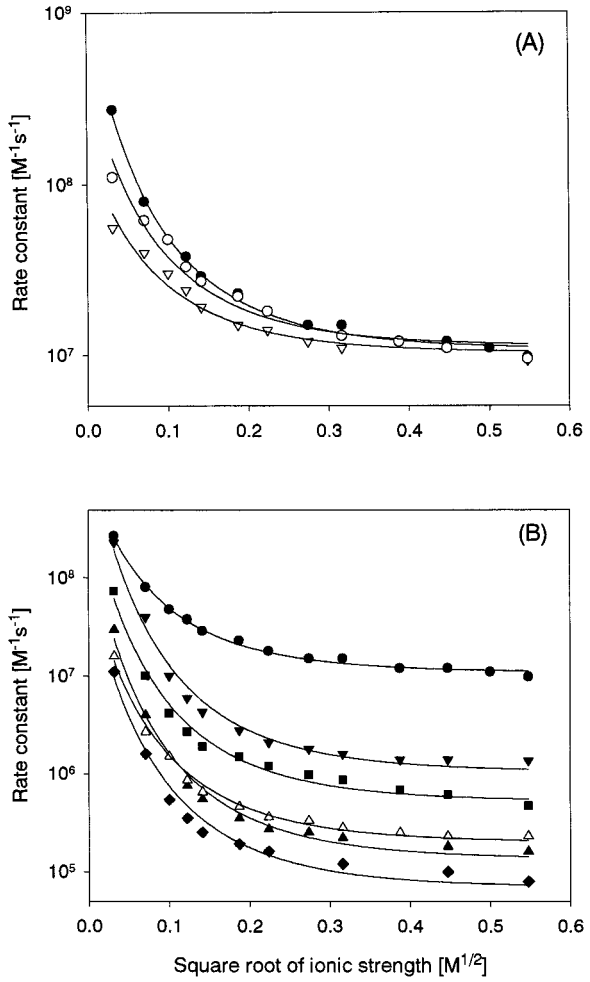

FIGURE 3: Ionic strength dependence of the observed second-order rate constants for the reaction of *Rvi. gelatinosus* HiPIP with wild-type and mutated tetraheme subunits of *Rvi. gelatinosus* RC. In panel A, symbols represent the values for wild-type (●), E79K (○), and E79K/E85K/E93K (▽). In panel B, symbols represent the values for wild-type (●), R72E (▼), L96K (■), V67E (▲), V67K (△), and V67E/R72E (◆). The solid lines correspond to fits of the data using the parallel plate (Watkins) model for protein−protein interactions (*28*). In each fit, the radius of the interaction site was taken as 19 Å (the wild-type value). The values of the parameter V_{ii} were the following: −4.6 (wild-type), −3.7 (E79K), −2.8 (E79K/E85K/E93K), −7.6 (R72E), −7.0 (L96K), −7.6 (V67E), −6.2 (V67K), −7.2 (V67E/R72E).

lower than the wild-type value. Next in order, L96K ($k_\infty = 5.2 \times 10^5$ M^{-1} s^{-1}) was followed by two mutants at position V67 ($k_\infty = 1.3 \times 10^5$ M^{-1} s^{-1} for V67E and 2.0×10^5 M^{-1} s^{-1} for V67K). The last was double mutant V67E/R72E, with the lowest value of $k_\infty = 7.0 \times 10^4$ M^{-1} s^{-1}. Apparently, the higher ionic strength intensified the differences between these mutants and the wild-type observed under conditions of low ionic strength.

RC Mutants in the Reaction with Rcy. tenuis HiPIP. The crystal structure of *Rvi. gelatinosus* HiPIP is not known and can only be predicted from the amino acid sequence comparison with HiPIPs that have already been crystallized (see the model shown in Figure 1b). HiPIP from *Rcy. tenius*, which belongs to the group of HiPIPs of known 3-D structure (*26*) (Figure 1c), was shown to be an efficient physiological electron donor to the RC-bound cytochrome subunit (*29*). Therefore, we used *Rcy. tenuis* HiPIP for comparative purposes and analyzed its kinetic behavior in the reaction with wild-type and all RC mutants.

Rcy. tenuis HiPIP reacted with wild-type *Rvi. gelatinosus* RCs with the second-order rate constant of 8.0×10^6 M^{-1} s^{-1} (Table 1). *Rcy. tenuis* HiPIP showed a marked ionic strength dependence, giving the value of infinite rate constant of 1.3×10^6 M^{-1} s^{-1} (Table 1). As summarized in Table 1, the mutations resulted in more or less severe inhibition of the electron transfer in a manner comparable to the effects observed in the case of *Rvi. gelatinosus* HiPIP. Some differences are described and discussed later.

RC Mutants in the Reaction with Horse Mitochondrial Cytochrome c. The replacements of negatively charged residues from the region near heme 1 (at positions E85, E79, E93, and D46) with positively charged ones have been shown to inhibit the reaction with horse cytochrome *c* (*10*). As shown in Figure 4A, a similar effect was observed for other mutations introducing positive charge: V67K, Q57K, and L96K. The extent of the inhibition was site-specific: the reduction of bound cytochrome, which occurs with the second-order rate constant of 4.5×10^6 M^{-1} s^{-1} in the wild-type, occurred with the rates of 2.0×10^6 M^{-1} s^{-1} in Q57K, 1.0×10^6 M^{-1} s^{-1} in V67K, and 3.4×10^5 M^{-1} s^{-1} in L96K.

On the other hand, the acceleration of the reaction rate was observed when negatively charged residues were introduced in the domain. The replacement of residues V67

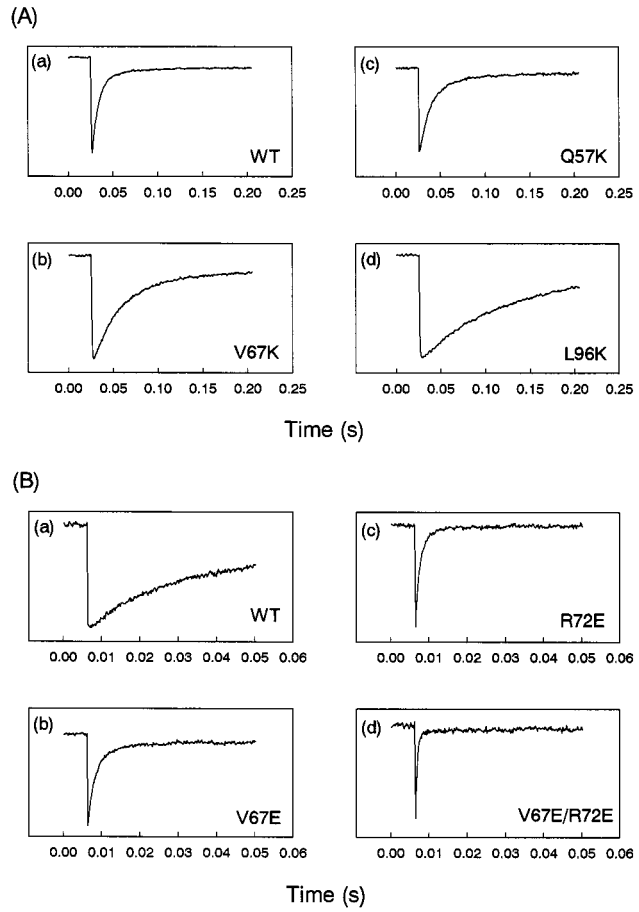

FIGURE 4: Single-flash-induced oxidation and reduction of RC-bound hemes measured at 556 nm for the reaction of wild-type (a) and mutated (b−d) tetraheme cytochrome subunits of *Rvi. gelatinosus* RC with horse mitochondrial cytochrome *c*. The concentration of cytochrome *c* was 40 μM (part A) or 13 μM (part B). The height of each panel corresponds to ΔABS of 1.8×10^{-3}. Buffer solution contained 2 mM Tris-HCl (pH 8), 20 μM DAD, and 0.1 mM sodium ascorbate.

and R72 with glutamates significantly improved the reactivity of mutated RCs with cytochrome *c* (Figure 4B): mutants V67E and R72E reacted with a second-order rate constant of 3.8×10^7 and 7.0×10^7 M^{-1} s^{-1}, respectively. Moreover, the reaction was further accelerated in the double mutant V67E/R72E which reacted with the rate of 2.1×10^8 M^{-1} s^{-1}. Apparently, the efficiency of the RC−cytochrome *c* interaction, in contrast to the RC−HiPIP interaction, strongly depends on the sign of the mutationally introduced charge.

In Figure 5, the second-order rate constants for the wild-type and the mutants at positions L96, V67, and R72 are plotted as a function of ionic strength. The effects of ionic strength confirm the strong dependence of the RC−cytochrome *c* interaction on the magnitude of negative charge exposed in the region of the binding domain on the cytochrome subunit. The mutants with additional negative charge in the interaction domain (V67E, R72E, and V67E/R72E) exhibit more profound ionic strength dependence with respect to the wild-type. This can be interpreted as reflecting the reaction involving a higher number of interacting charges. The mutants with additional positive charge (V67K and L96K) show significant reductions of ionic strength dependence. These effects are within the range of decrease previously observed for the mutants having positive charge at positions E85, E79, E93, and D46 (*10*) and are

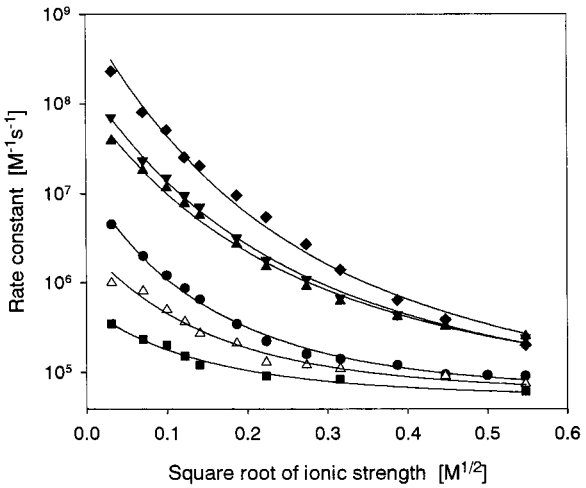

FIGURE 5: Ionic strength dependence of the observed second-order rate constants for the reaction of horse mitochondrial cytochrome *c* with wild-type and mutated tetraheme subunits of *Rvi. gelatinosus* RC. Symbol code is the same as in Figure 3: wild-type (●), L96K (■), V67K (△), V67E (▲), R72E (▼), and V67E/R72E (◆). The solid lines correspond to fits of the data using the same model as in Figure 3. For optimal fits, the radius of the interaction site was taken as 10.4 Å (for the wild-type, L96K, V67K) or 6 Å (for V67E, R72E, V67E/R72E). The values of the parameter V_{ii} were the following: −5.5 (wild-type), −2.3 (L96K), −3.8 (V67K), −7.4 (V67E), −8.0 (R72E), −9.8 (V67E/R72E).

indicative of partial loss of attractive interactions in the binding domain.

Comparing the effects of two oppositely charged mutants at position V67, it should be noted that the extent of the acceleration caused by V67E appears to be larger than the inhibition caused by V67K. It should be noted as well that all mutants shown in Figure 5 displayed similar behavior at the region of high ionic strength and had similar values of rate constant at infinite ionic strength (the values of k_∞ ranged from 5.2×10^4 to 7.0×10^4 M^{-1} s^{-1}). This is in sharp contrast to the ionic strength dependence of these mutants in the reaction with *Rvi. gelatinosus* HiPIP (note that the set of mutants in Figure 5 is exactly the same as that in Figure 3B).

Mapping the Binding Site for HiPIP and Cytochrome c. The contribution of each tested residue of the cytochrome subunit to the binding of HiPIP and cytochrome *c* was evaluated by calculating the degree of inhibition caused by single mutations at individual positions expressed as $i = [\log(k_{wt}/k_m) + \log(k_{\infty wt}/k_{\infty m})]/n$, where k_{wt} and k_m are second-order rate constants at low ionic strength (2 mM Mops-NaOH for HiPIP, 2 mM Tris-HCl for cytochrome *c*) of wild-type and mutant, respectively; $k_{\infty wt}$ and $k_{\infty m}$ are second-order rate constants at infinite ionic strength of wild-type and mutant, respectively, and *n* is net charge change caused by mutation (taken as 1 or 2, depending on the introduced mutation). From the set of data obtained for each soluble electron donor, the largest inhibition (largest value of *i* parameter) was normalized to 100% (position V67 in the case of HiPIP, or L96 in the case of cytochrome *c*), and the relative percentages of inhibition for the remaining positions were calculated accordingly. The results are shown in Figure 6. In Figure 7, the data from Figure 6 for *Rvi. gelatinosus* HiPIP and cytochrome *c* are projected onto the model of 3-D structure of the cytochrome subunit to visualize the positions of the binding sites.

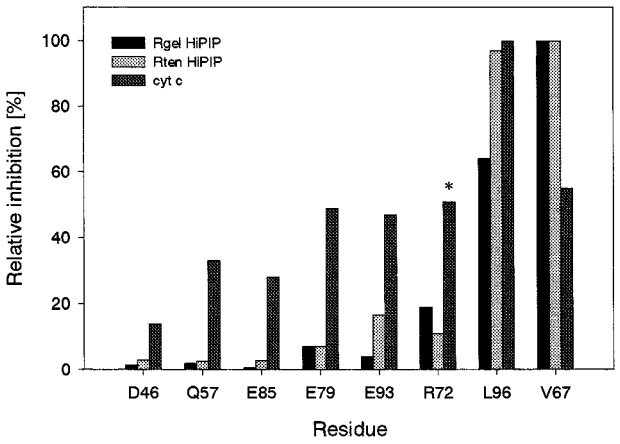

FIGURE 6: Comparison of the effects of individual mutated positions in *Rvi. gelatinosus* RC-bound tetraheme cytochrome subunit on the reactivity of *Rvi. gelatinosus* HiPIP (black bars), *Rcy. tenuis* HiPIP (light gray bars), and horse mitochondrial cytochrome *c* (dark gray bars). The percent of relative inhibition given by the bars was estimated as described in Results. Asterisk indicates a value obtained from the effect of acceleration of the reaction with cytochrome *c* in the mutant R72E (note that in the case of cytochrome *c* the acceleration was also observed in the mutant V67E (76%), but a value given by the bar (55%) shows the inhibition caused by V67K).

DISCUSSION

Identification of the Residues Forming the Binding Site for HiPIP. In previous studies, we identified the region around the solvent-exposed edge of low-potential heme 1 of the RC-bound tetraheme cytochrome subunit as a binding site for soluble cytochromes and HiPIP (*10*, *11*). In the case of HiPIP, the identification was based on the observation that the electron-transfer reaction between this protein and the RC is significantly impaired in two RC mutants: the single mutant V67K and the triple mutant E79K/E85K/E93K (*11*). In this study, we confirm this finding by showing that other mutations near heme 1 inhibit the reaction as well. Furthermore, the site specificity of the inhibition observed for individual mutations allows us now to predict more precisely which amino acids form the encounter surface.

The strongest inhibition observed for the mutations of valine at position 67 (V67K and V67E) indicates that the region close to heme 1, in the vicinity of this residue, is dominantly involved in the binding of HiPIP (Figure 7b). Consistent with that idea, a severe impairment of the interaction with HiPIP was also observed for the mutations at two other positions in the region near heme 1: L96K and R72E. In contrast to these three positions, the replacement of other residues had a less pronounced effect on the reactivity of HiPIP or no effect at all. These positions included a cluster of negatively charged acidic residues E79, E85, E93, and D46, and one uncharged residue Q57. While the electron-transfer rate from HiPIP remained almost unaltered in the case of D46H, Q57K, and E85K, slight inhibitory effects were recognized in the case of E79K and E93K. This was further confirmed by the effects of multiple mutations. In particular, the fact that the triple mutant E79K/E85K/E93K showed clear inhibition at low ionic strength (apparent additivity of E79K and E93K) indicates that both E79 and E93 contribute to the binding to a certain degree. It should be noted, however, that the extent of inhibition caused by the mutations at positions E79 and E93 is much smaller than would be expected if these residues were to form salt bridges in the transient complex with HiPIP (see the comparison with soluble cytochrome *c* below). It is therefore possible that these residues are located in the peripheral region of the HiPIP-binding site and only facilitate the initial recognition process without participating in the final docking.

Comparison of the Binding Sites for HiPIP and Cytochrome c: Implications for Different Docking Mechanisms. From the comparison shown in Figures 6 and 7, it is apparent that the cytochrome-*c*-binding site occupies a much larger area of the subunit than the HiPIP-binding site. The encounter surface for cytochrome *c* is definitely covered by E79, E93, V67, and R72, all of which surround the solvent-exposed edge of heme 1, forming a ring of approximately 24 Å diameter. In addition, even the residues located more distantly from the heme edge and/or beyond the frontal surface (D46, E85, and Q57) appear to contribute significantly to the binding. This is in contrast to the HiPIP-binding site, which appears to be restricted only to the small region with V67, R72, and L96 (approximately 12 Å diameter) in addition to peripherally located E79 and E93. Other residues (D46, Q57, and E85) showing no contribution to the binding seem to be located entirely outside the border of this encounter surface. Interestingly, the comparison of the relative contribution of V67 and L96 (Figures 6 and 7b) to the binding of HiPIP suggests that the left side of heme 1 (as viewed in Figure 7) is more dominantly involved in the binding than the right side. This seems to be further supported by a difference in the effects of L96K and E93K, which appears to be very large despite the short distance between the residues. The residues forming the cytochrome-*c*-binding site are more uniformly distributed on both sides of the heme crevice (Figure 7a).

The most noticeable distinction between the HiPIP-binding region and the cytochrome-*c*-binding region is the relative contribution of the acidic cluster (D46, E79, E85, and E93). As shown here and in a previous study (*10*), negatively charged residues forming this cluster are critically important for the recognition of cytochrome *c*. Not only did all introduced positive charges in the region around heme 1 inhibit the reaction with cytochrome *c* but also negative charges additionally introduced to the region accelerated the reaction rate (Figures 4 and 5). This clearly indicates that favorable electrostatic attractions between the acidic residues of the RC and the lysines of cytochrome *c* primarily control the recognition between these two proteins. Moreover, the observation that the acceleration of the reaction rate in the mutant V67E was larger than the inhibition caused by the oppositely charged mutation at the same position (V67K) suggests that the uniform distribution of charged residues around the redox center may have an additional advantage in facilitating the formation of the transient complex. This agrees with the structure of cytochromes c_2, which usually possess several positively charged residues encircling the heme crevice. Corresponding to this, in species where these cytochromes are the only electron donors to the RC, the negatively charged residues can be found on both sides of heme 1 of the cytochrome subunit. This is the case in *Blc. viridis* in which the tetraheme cytochrome subunit has glutamates at positions 67 and 48 (on the left side of heme 1, as viewed in Figure 1a) in addition to E93, E85, and E79 (on the right side and the bottom of heme 1). Similar

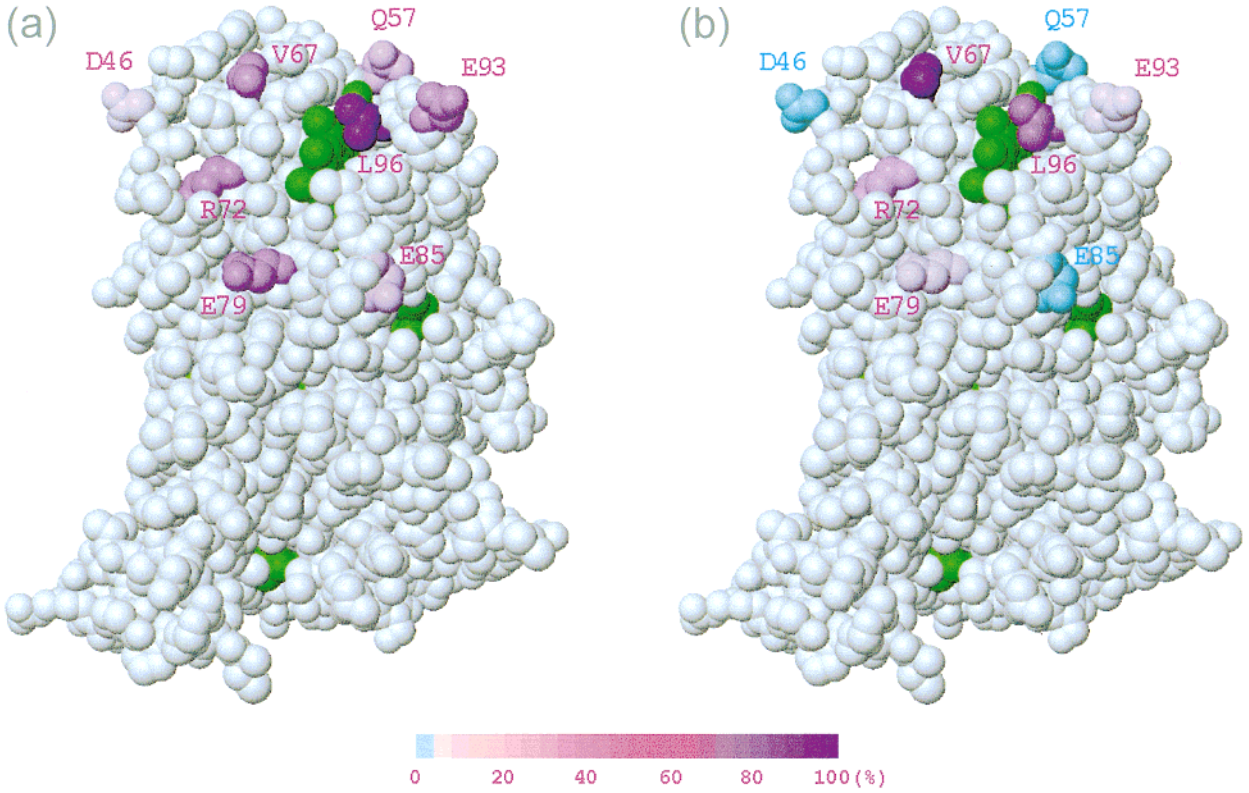

FIGURE 7: Schematic map of the binding site for cytochrome *c* (a) and HiPIP (b) on the surface of the tetraheme cytochrome subunit of *Rvi. gelatinosus* RC. The orientation of the molecule is the same as in Figure 1a. The relative contributions of tested by mutation residues are compared using a violet intensity scale (color intensity corresponds to the degree of inhibition shown in Figure 6). The observable lack of contribution is shown in blue. Hemes are green. The figure was generated using the programs MOLSCRIPT (*56*) and RASTER3D (*57*).

distribution of acidic residues is also predicted in *Rhodospirillum molischianum* and *Rhodobium marinum* (*30*).

In *Rvi. gelatinosus*, the acidic cluster surrounding heme 1 lacks negative charges on the left side of its edge (Figure 1a): positions 67 and 48 are occupied by uncharged valine and serine, respectively, and the only charged residue in this region, D46, is located somewhat distantly from the heme. The uncharged and hydrophobic residues in the region close to the exposed edge of heme 1 appear to be critically important for the binding of HiPIP, while the contribution of the acidic cluster itself is rather minor (Figures 6 and 7b). These observations suggest that the molecular recognition between HiPIP and the RC is primarily controlled by hydrophobic interactions between nonpolar residues rather than by electrostatic interactions between oppositely charged residues.

In support of this idea, the fact that oppositely charged mutations at position V67 (V67E and V67K) have similar inhibitory effects on the reactivity of HiPIP emphasizes the importance of the uncharged character of valine at this place. This can be contrasted with the behavior of cytochrome *c*, the reactivity of which shows a clear dependence on the sign of the introduced charge (opposite effects of V67E and V67K).

Furthermore, the ionic strength dependency of the reaction of HiPIP with some of the RC mutants differs from the pattern anticipated for the electrostatic mode of interaction. In the case of cytochrome *c*, the reaction rates of all mutants converged to the value of wild-type (Figure 5), indicating that the mutations affected mostly the electrostatic characteristics of RC−cytochrome *c* interaction. In the assays with HiPIP, the mutants at positions V67, L96, and R72 displayed a profound site-specific decrease of the reaction rates both at low and high ionic strength (Figure 3B). These sharp decreases in reactivity do not seem to reflect the impairment of electrostatic interactions between two proteins. Considering the positions of V67, L96, and R72 with respect to the hydrophobic core near heme 1 (Figure 1a), these effects seem to be related with the hydrophobic character of the HiPIP binding domain.

The proposed importance of the hydrophobic interactions in the binding of HiPIP has to be reconciled with the strong ionic strength dependency observed for the reaction between the wild-type RC and HiPIP. Such a dependency is usually taken as evidence for the binding controlled mainly by favorable electrostatic attractions (*5*−*7*, *9*, *10*, *17*, *28*, *31*). However, the mutations of all charged positions which may participate in the electrostatic recognition between the RC and HiPIP through the formation of salt bridges resulted in a little or no change in the ionic strength dependency with respect to the wild-type [note that these mutations severely diminished the ionic strength dependency of cytochrome *c* (*10*)]. In particular, the dependence that remained after the introduction of the triple substitution E79K/E85K/E93K (Figure 3A), which replaced most of the charged residues in the region around heme 1, can hardly be ascribed as reflecting the simple plus-minus electrostatic interactions. In addition, the large value of the radius of the interaction site

(19 Å) required to fit the wild-type data does not seem to correspond to the size of the site revealed through mutagenesis experiments (a radius of approximately 6 Å). A similar value (20 Å) was obtained for the reaction of *Rhodoferax fermentants* HiPIP with the RC (*32*). These large experimental estimates suggest that the ionic strength dependency of the HiPIP reaction does not reflect, at least solely, the electrostatic mode of interaction. As far as the electrostatic component is concerned, its possible contribution may derive from the complementarity of the delocalized electrostatic potentials of the encounter surfaces of HiPIP and the RC, according to the mechanism proposed by Tiede et al. (*33*).

It should be noted that some of the mutations used in this study may provide steric hindrance for the interaction with soluble partners. In particular, this is likely to occur in mutant L96K, which has an alteration at the closest position to the heme edge in front of the encounter surface (Figure 1a). The inhibition caused by L96K is very strong in the case of both HiPIP and cytochrome *c*, and the effect of L96K on the reactivity of cytochrome *c* is larger than would be expected for a change of one charge in the interaction domain (see comparison with V67K in Figure 6). This suggests that the structure of the hydrophobic pocket immediate to heme 1 is important for proper coupling of the proteins and may allow some hydrophobic contacts to occur even when the reaction is primarily controlled by electrostatic forces. On the other hand, all other mutations encircling heme 1 with a reasonable distance from its edge, influenced the binding of cytochrome *c* according to theoretical predictions, i.e., they inhibited or accelerated the reaction rate in the range consistent with the sign and magnitude of the introduced charge. This indicates that, for the reaction with cytochrome, the local steric effects of mutations at these positions were minor with respect to the electrostatic effects caused by the change in charge.

Putative Docking Region on HiPIP, Model of Binding. The model of *Rvi. gelatinosus* HiPIP shows a hydrophobic zone occupying the surface surrounding the iron−sulfur cluster (Figure 1b). This side of the molecule can be considered as a possible region involved in the recognition of the hydrophobic domain of the bound cytochrome subunit. Results from the comparative analysis of the 15 known HiPIP amino acid sequences support this idea (*23*). The same side of the protein (as viewed in Figure 1, panels b and c), referred to as the front side, appears to be well-conserved in all HiPIPs showing high conservation of the hydrophobic residues. This side is, therefore, the most likely part involved in molecular recognition processes (*23*).

The front side of the model of *Rvi. gelatinosus* HiPIP does not show a ring of positively charged residues encircling the redox center. Instead, the lysine residues accumulate only at the right edge (as viewed in Figure 1b) and in the upper part. This asymmetric charge distribution may correlate in some way with the negative charge near heme 1 of the subunit (the right side of the heme cleft seen in Figure 1a is more negative than the left side). However, the role of charged residues of HiPIP in its binding to the RC seems to be supplementary in light of the results of mutagenesis in the RC counterpart. These charged residues may serve a more important function when HiPIP binds to the cytochrome bc_1 complex, its physiological electron donor (*18*).

The front side of the 3-D structure of *Rcy. tenuis* HiPIP resembles that of *Rvi. gelatiosus* HiPIP in that it possesses a similar hydrophobic domain (Figure 1c). Thus, it is not surprising that the inhibitory effects of the mutations in the region around heme 1 of the subunit in the reaction with *Rcy. tenuis* HiPIP are generally comparable with the effects observed with *Rvi. gelatinosus* HiPIP. However, the relative contribution of the electrostatic component in the *Rcy. tenuis* HiPIP−RC interaction appears to be larger in comparison with *Rvi. gelatinosus* HiPIP−RC interaction. This is indicated by the stronger inhibition in the single mutant E93K (Figure 6) and the relatively smaller ionic strength dependency of the triple mutant E79K/E85K/E93K (Table 1) observed in *Rcy. tenuis* reactions.

Considering the possible orientations of *Rvi. gelatinosus* HiPIP or *Rcy. tenuis* HiPIP docked in the RC, it can be suggested that the right (charged) side of the HiPIP molecule (as viewed in Figure 1, panels b and c) aligns itself toward the region around E79 and E93 with close interaction between the hydrophobic domains of HiPIP and the cytochrome subunit. Such orientation modeled for *Rcy. tenuis* HiPIP is shown in Figure 8. In this model, the distance between the edge of heme 1 and the iron−sulfur cluster is approximately 7 Å. The residues engaged in the hydrophobic interactions are F56, V67, and L96 of the cytochrome subunit and F10 and V42 of *Rcy. tenuis* HiPIP (Figures 1, panels a and c, and 8). In the case of *Rvi. gelatinosus* HiPIP (model not shown), the interacting positions are L13 and L55 (Figure 1b). In both cases, the C-terminus of HiPIP (K61 and K62 for *Rcy. tenuis* HiPIP, or K72 and K73 for *Rvi. gelatinosus* HiPIP) remains somewhat distant from the surface around E79, supporting experimental indications that this region may not participate in the final docking of HiPIP. In this respect, the modeled orientation of HiPIP molecule differs from the orientation of cytochrome c_2 predicted for the RC-cytochrome c_2 interaction in *Blc. viridis* (see Figure 8 in ref *10*). In the latter model, cytochrome c_2 is shifted slightly down from the top of the cytochrome subunit (as viewed in Figure 8), resulting in closer contacts between cytochrome c_2 and the region around E79 (possible salt bridge between E79 of the cytochrome subunit and K78 of cytochrome c_2).

The proposed configuration of the complex with *Rcy. tenuis* HiPIP places its K41 near E93 of the subunit. This additional charge on the surface of *Rcy. tenuis* HiPIP (note that the corresponding bottom of *Rvi. gelatinosus* HiPIP lacks any charged residues) may be partly responsible for the larger contribution of the electrostatic component in the binding of *Rcy. tenuis* HiPIP to the RC and account for the observed differences in the kinetic behavior of both HiPIPs in their reactions with E93K (Figure 6).

In the docking model of RC−HiPIP interaction, the contact area of the solvent-accessible surface of the RC is reduced to less than half (approximately 30%) in comparison with the same area in the model proposed for RC−cytochrome c_2 interaction (*10*). This agrees with the observations that the binding site for HiPIP is smaller than the cytochrome-*c*-binding site (Figure 7).

Evolution of Electrostatic and Hydrophobic Components of the Binding Domain. The region around the solvent-exposed heme 1 of the cytochrome subunit provides two different structural domains: a cluster of negatively charged acidic residues encircling the heme crevice and a hydrophobic domain inside this cluster (mostly the left side as viewed in Figure 1a). The results with mutated RCs showed that

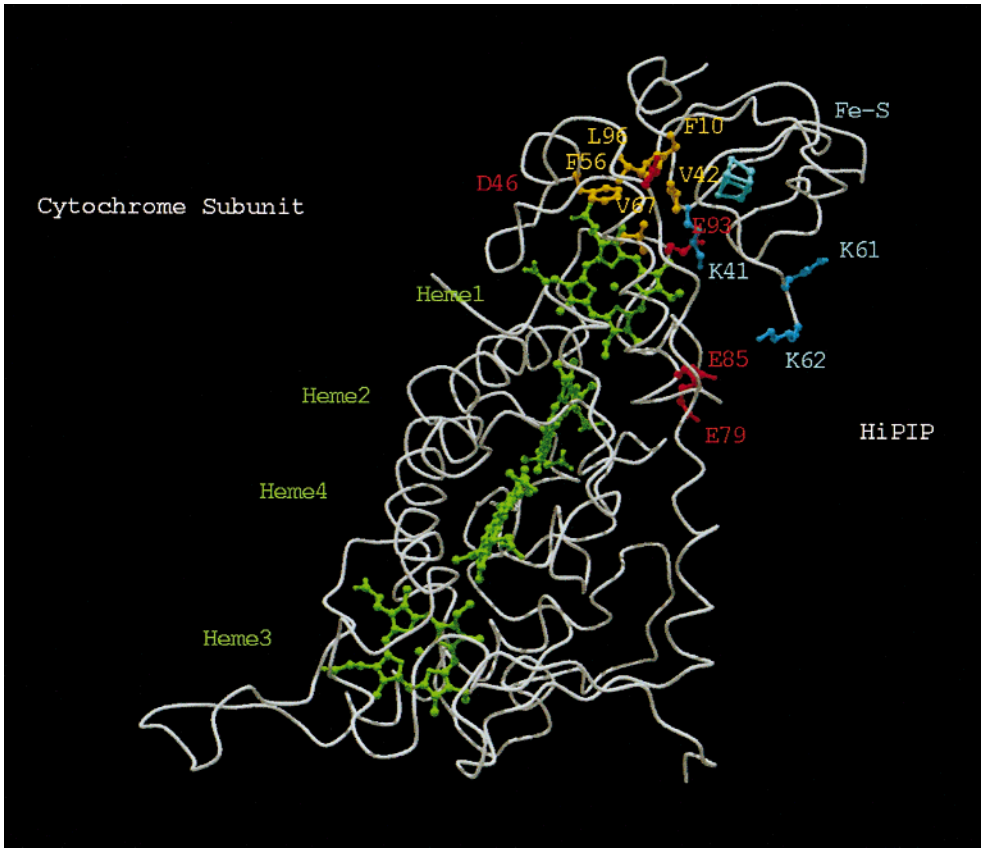

FIGURE 8: Model of possible interaction between the cytochrome subunit of the *Rvi. gelatinosus* RC (left) and *Rcy. tenuis* HiPIP (right). Thread drawings based on the α-carbon positions are colored white. The side-chain atoms of the charged residues are shown as ball-and-stick models in blue (lysines) and red (glutamates, aspartate). The side-chain atoms of hydrophobic residues are shown in yellow. The heme atoms and the iron−sulfur cluster are also shown as ball-and-stick models in green and cyan, respectively. The figure was generated using the programs MOLSCRIPT (*56*) and RASTER3D (*57*).

both components are important in the binding of soluble partners of the RC, although the contribution of an electrostatic component and a hydrophobic component varies depending on the particular interaction. In the case of the complex formed between *Rvi. gelatinosus* RC and *Rvi. gelatinosus* HiPIP the hydrophobic domain of heme 1 appears to be of primary importance, while the contribution of the acidic cluster is rather minor. The interactions of *Rvi. gelatinosus* RC with mitochondrial cytochrome *c* and *Blc. viridis* cytochrome c_2 are predominantly controlled by electrostatic favorable attractions (formation of salt bridges), whereas the interaction with *Rcy. tenuis* HiPIP appears to be stabilized by both hydrophobic and electrostatic interactions. Electrostatics is important in the binding of *Rvi. gelatinosus* cytochrome c_8, although this interaction seems to involve less charge and is presumably also controlled by hydrophobic forces (*10*, unpublished observations).

It is natural to expect that the structures of the binding domains are optimized so that the physiological protein partners mediate the most efficient electron transfer. The results of this study showed that some mutations in the *Rvi. gelatinosus* cytochrome subunit can modify the electron-donor-binding site in such a way that the physiological interaction (with HiPIP) is significantly impaired, while the nonphysiological interaction (with soluble cytochrome *c*) is considerably improved and its effectiveness in vitro can even correspond to the level of physiological interaction. These effects, observed for mutations V67E, R72E, and V67E/R72E, are apparently connected with the change in the electrostatic and hydrophobic component of the interaction domain. In other words, an additional negative charge facilitates the electrostatic recognition of cytochrome *c* but at the same time destroys the effectiveness of the hydrophobic coupling with HiPIP. In this context, it seems possible that the evolutionary pathway leading to the most effective interactions between the RC and donor proteins involved structural adjustments of both electrostatic and hydrophobic domains at the interface. As a result, the relative contribution of the electrostatic and hydrophobic component in the RC−donor protein interaction may vary in different species of photosynthetic bacteria.

From this perspective, it is possible to explain the kinetic behavior of the *Blc. viridis* tetraheme subunit in the reaction with different donor proteins (*31*). Its putative binding domain (the region around heme 1) has, in comparison with the binding domain on the *Rvi. gelatinosus* tetraheme subunit, a more highly developed electrostatic component (additional glutamates at positions 67 and 48) at the expense of the hydrophobic component. In light of the results with mutants at positions 67 and 72, this difference can make the *Blc. viridis* domain much more efficient in the binding of cytochromes (including physiological cytochrome c_2) than in the binding of HiPIPs, which was indeed observed experimentally (*31*).

Role of Low-Potential Hemes of the Cytochrome Subunit. Despite extensive studies on the structural and kinetic

properties of RC-bound tetraheme cytochrome subunits in various species, the functional significance of the characteristic "high-low-high-low potential" arrangement of its four hemes is still a matter of debate. In particular, the role of the low-potential hemes and the significance of the interposition of one of them (heme 4) between two high-potential hemes are still not fully understood (*1*, *34*, *35*).

Considering that the region around the exposed edge of heme 1 of the *Rvi. gelatinosus* cytochrome subunit shows capability to bind two different types of bacterial soluble electron donors to the RC (cytochrome *c* and HiPIP), it seems reasonable to assume that this region is a general site of interaction for all RC-bound tetraheme cytochromes and all four hemes, including low-potential ones, are involved in the electron flow toward P^+. In this context, an interesting exception has recently been found in *Rhodovulum sulfidophilum*, a species which possesses a three-heme cytochrome subunit bound to the RC (*36*). In this so far unique cytochrome, heme 1 (the most distant heme from P, corresponding to heme *c*-554 in *Blc. viridis*) is deleted, while heme 2 (the next after heme 1, corresponding to heme *c*-556 in *Blc. viridis*) lacks the sixth ligand for the heme iron. Therefore, it seems likely that, in *Rdv. sulfidofilum*, only the two hemes closest to P are involved in the electron flow toward P^+, utilizing a binding site for soluble electron donor different from that of tetraheme cytochromes. This implies that the binding site in this species may be shifted by two hemes from the outermost heme 1 of tetraheme cytochromes. *Rdv. sulfidofilum* is closely related to the *Rhodobacter* species (*37*), a group having the RC without a bound cytochrome subunit, and can be considered as an evolutionary step toward a complete deletion of the subunit (*1*, *3*, *38*).

Relevance to Other Electron-Transfer Complexes. The hydrophobic mode of interaction between the RC and HiPIP proposed for *Rvi. gelatinosus* differs from the general mechanism of RC−cytochrome c_2 interaction and cytochrome bc_1−cytochrome c_2 interaction, which considers electrostatic forces as a major contributor to the formation of electron-transfer complex (*5*−*7*, *9*, *10*, *17*, *31*, *39*−*41*). However, the *Rvi. gelatinosus* RC is not the sole example of a protein utilizing the hydrophobic domain in the interaction with a physiological partner. Several other protein−protein interactions in both photosynthetic and nonphotosynthetic electron-transfer systems have been found to be mediated by hydrophobic forces. A particular analogy to the RC−HiPIP interaction can be seen in the systems in which plastocyanin acts as a mobile electron carrier between cytochrome *f* and PS I. Plastocyanin, which has two distinct interaction sites, one close to the copper (hydrophobic patch), and the other one remote from the copper (acidic patch), appears to use the former site for interaction with P700 of PS I (*42*−*44*). This suggests that hydrophobic contacts are important, if not dominant, in the formation of the plastocyanin−PSI complex (*45*). A functional analogue of plastocyanin in cyanobacteria and some algae, cytochrome c_6, is another protein likely to use a hydrophobic domain in molecular recognition processes. In the 3-D structure of this protein, the region favorable for electron transfer (close to the heme crevice) is mostly hydrophobic and distant from the negatively charged zone (*46*). A hydrophobic mode of interaction was also proposed for the interaction of azurin (closely related in structure to plastocyanin) with nitrate reductase and cytochrome *c*-551 (*47*). Another example is provided by the cocrystal structures of cytochrome *c* peroxidase−cytochrome *c* (*48*) and methylamine dehydrogenase−amicyanin (*49*, *50*), which show that the interaction between proteins in these complexes occurs mainly through the hydrophobic interface.

Cases of interchangeability between different electron carriers performing the same function have been reported for several in vivo electron-transfer systems [for example HiPIP/cytochrome c_8 (*29*, *51*), plastocyanin/cytochrome c_6 (*52*−*54*)], raising questions about the molecular basis of protein−protein recognition in such systems and the evolution of the binding mechanisms (*55*). We showed that in *Rvi. gelatinosus* RC, the mainly hydrophobic interaction region with HiPIP almost completely overlaps with the mostly electrostatic interaction region with cytochrome *c*. This particular feature makes the single binding region on a membranous protein complex capable of anchoring two very different types of soluble electron donor proteins.

REFERENCES

1. Nitschke, W., and Dracheva, S. M. (1995) in *Anoxygenic Photosynthetic Bacteria* (Blankenship, R. E., Madigan, M. T., and Bauer, C. E., Eds.) pp 775−805, Kluwer Academic, Dordrecht, The Netherlands.
2. Meyer, T. E., and Donohue, T. J. (1995) in *Anoxygenic Photosynthetic Bacteria* (Blankenship, R. E., Madigan, M. T., and Bauer, C. E., Eds.) pp 725−745, Kluwer Academic, Dordrecht, The Netherlands.
3. Matsuura, K. (1994) *J. Plant Res. 107*, 191−200.
4. Bartsch, R. G. (1991) *Biochim. Biophys. Acta 1058*, 28−30.
5. Hall, J., Zha, X., Durham, B., O'Brien, P., Vieira, B., Davis, D., Okamura, M., and Millett, F. (1987) *Biochemistry 26*, 4494−4500.
6. Hall, J., Ayres, M., Zha, X., O'Brien, P., Durham, B., Knaff, D. B., and Millett, F. (1987) *J. Biol. Chem. 262*, 11046−11051.
7. Long, J. E., Durham, B., Okamura, M., and Millett, F. (1989) *Biochemistry 28*, 6970−6974.
8. Adir, N., Axelrod, H. L., Beroza, P., Isaacson, R. A., Rongey, S. H., Okamura, M. Y., and Feher, G. (1996) *Biochemistry 35*, 2535−2547.
9. Caffrey, M. S., Bartsch, R. G., and Cusanovich, M. A. (1992) *J. Biol. Chem. 267*, 6317−6321.
10. Osyczka, A., Nagashima, K. V. P., Sogabe, K., Miki, K., Yoshida, M., Shimada, K. and Matsuura, K. (1998) *Biochemistry 37*, 11732−11744.
11. Osyczka, A., Nagashima, K. V. P., Shimada, K., and Matsuura, K. (1999) *Biochemistry 38*, 2861−2865.
12. Hiraishi, A. (1997) *Int. J. Syst. Bacteriol. 47*, 217−219.
13. Deisenhofer, J., Epp, O., Miki, K., Huber, R., and Michel, H. (1985) *Nature 318*, 618−624.
14. Deisenhofer, J., and Michel, H. (1989) *EMBO J. 8*, 2149−2170.
15. Deisenhofer, J., Epp, O., Sinning, I., and Michel, H. (1995) *J. Mol. Biol. 246*, 429−457.
16. Nagashima, K. V. P., Matsuura, K., Ohyama, S., and Shimada, K. (1994) *J. Biol. Chem. 269*, 2477−2484.
17. Knaff, D. B., Willie, A., Long, J. E., Kriauciunas, A., Durham, B., and Millett, F. (1991) *Biochemistry 30*, 1303−1310.
18. Schoepp, B., Parot, P., Menin, L., Gaillard, J., Richaud, P., and Verméglio, A. (1995) *Biochemistry 34*, 11736−11742.
19. Osyczka, A., Yoshida, M., Nagashima, K. V. P., Shimada, K., and Matsuura, K. (1997) *Biochim. Biophys. Acta 1321*, 93−99.
20. Bartsch, R. G. (1978) *Methods Enzymol. 53*, 329−340.
21. Matsuura, K., and Shimada, K. (1986) *Biochim. Biophys. Acta 852*, 9−18.
22. Benning, M. M., Meyer, T. E., Rayment, I., and Holden, H. M. (1994) *Biochemistry* 33, 2476−2483.

23. Van Driessche, G., Ciurli, S., Hochkoeppler, A., and Van Beeumen, J. J. (1997) *Eur. J. Biochem. 244*, 371−377.
24. Kerfeld, C. A., Salmeen, A. E., and Yeates, T. O. (1998) *Biochemistry 37*, 13911−13917.
25. Müller, K., Ammann, H. J., Doran, D. M., Gerber, P. R., Gubernator, K., and Schrepfer, G. (1989) *Prog. Clin. Biol. Res. 291*, 219−226.
26. Rayment, I., Wasenberg, G., Meyer, T. E., Cusanovich, M. A., and Holden, H. M. (1992) *J. Mol. Biol. 228*, 672−686.
27. Connolly, M. L. (1983) *J. Appl. Crystallogr. 16*, 548−558.
28. Watkins, J. A., Cusanovich, M. A., Meyer, T. E., and Tollin, G. (1994) *Protein Sci. 3*, 2104−2114.
29. Menin, L., Schoepp, B., Parot, P., and Verméglio, A. (1997) *Biochemistry 36*, 12183−12188.
30. Nagashima, K. V. P., Sakuragi, Y., Shimada, K., and Matsuura, K. (1998) *Photosynth. Res. 55*, 349−355.
31. Meyer, T. E., Bartsch, R. G., Cusanovich, M. A., and Tollin, G. (1993) *Biochemistry 32*, 4719−4726.
32. Hochkoeppler, A., Zannoni, D., Ciurli, S., Meyer, T. E., Cusanovich, M. A., and Tollin, G. (1996) *Proc. Natl. Acad. Sci. U.S.A. 93*, 6998−7002.
33. Tiede, D. M., Vashishta, A. C., and Gunner, M. R. (1993) *Biochemistry 32*, 4515−4531.
34. Nitschke, W., and Rutherford, A. W. (1994) *Biochem. Soc. Trans. 22*, 694−699.
35. Yoshida, M., Shimada, K., and Matsuura, K. (1999) *Plant Cell Physiol. 40*, 192−197.
36. Masuda, S., Yoshida, M., Nagashima, K. V. P., Shimada, K., and Matsuura, K. (1999) *J. Biol. Chem. 274*, 10795−10801.
37. Hiraishi, A., and Ueda, Y. (1994) *Int. J. Syst. Bacteriol. 44*, 15−23.
38. Matsuura, K., and Shimada, K. (1990) in *Current Research in Photosynthesis* (Baltscheffsky, M., Ed.) Vol. I, pp 193−196, Kluwer Academic, Dordrecht, The Netherlands.
39. Hall, J., Zha, X., Yu, L., Yu, C. A., and Millett, F. (1987) *Biochemistry 26*, 4501−4504.
40. Güner, S., Willie, A., Millett, F., Caffrey, M. S., Cusanovich, M. A., Robertson, D. E., and Knaff, D. B. (1993) *Biochemistry 32*, 4793−4800.
41. Hall, J., Kriaucionas, A., Knaff, D. B., and Millett, F. (1987) *J. Biol. Chem. 262*, 14005−14009.
42. Haehnel, W., Jansen, T., Gause, K., Klösgen, R. B., Stahl, B., Michl, D., Huvermann, B., Karas, M., and Herrmann, R. G. (1994) *EMBO J. 13*, 1028−1038.
43. Sigfridsson, K., Young, S., and Hansson, O. (1996) *Biochemistry 35*, 1249−1257.
44. Sigfridsson, K., Young, S., and Hansson, O. (1997) *Eur. J. Biochem. 245*, 805−812.
45. Sigfridsson, K. (1998) *Photosynth. Res. 57*, 1−28.
46. Kerfeld, C. A. (1997) *Photosynth. Res. 54*, 81−98.
47. Van de Kamp, M., Silvestrini, M. C., Brunori, M., Van Beeumen, J., Hali, F. C., and Canters, G. W. (1990) *Eur. J. Biochem. 194*, 109−118.
48. Pelletier, H., and Kraut, J. (1992) *Science 258*, 1748−1755.
49. Chen, L., Durley, R., Poliks, B. J., Hamada, K., Chen, Z., Mathews, F. S., Davidson, V. L., Satov, Y., Huizinga, E., Vellieux, F. M. D., and Hol, W. G. J. (1992) *Biochemistry 31*, 4959−4964.
50. Chen, L., Durley, R. C. E., Mathews, F. S., and Davidson, V. L. (1994) *Science 264*, 86−90.
51. Hochkoeppler, A., Ciurli, S., Kofod, P., Venturoli, G., and Zannoni, D. (1997) *Photosynth. Res. 53*, 13−21.
52. Wood, P. M. (1978) *Eur. J. Biochem. 87*, 9−19.
53. Ho, K. K., and Krogmann, D. W. (1984) *Biochim. Biophys. Acta 766*, 310−316.
54. Sandmann, G. (1986) *Arch. Microbiol. 145*, 76−79.
55. Hervás, M., Navarro, J. A., Díaz, A., Bottin, H. and De la Rosa, M. A. (1995) *Biochemistry 34*, 11321−11326.
56. Kraus, P. (1991) *J. Appl. Crystallogr. 24*, 946−950.
57. Merritt, E. A., and Murphy, M. E. P. (1997) *Acta Crystallogr., Sect. D 50*, 869−873.

BI990907D